Distribution of active tectonics in the Himalayan piedmont (Darjeeling, Eastern India) inferred from Horizontal-to-Vertical Spectral Ratio analysis of passive seismic records

Short title: Active tectonics in the Darjeeling piedmont

E. Large [a], P. Huyghe [a], J-L. Mugnier [b], B. Guillier [a], S. Taral [c], B.R. Gyawali [d] and T. Chabraborty [e]

[a] *Institut des Sciences de la Terre, Université Grenoble Alpes/CNRS, CS40700, 38058 Grenoble Cedex 9, France*

[b] *Institut des Sciences de la Terre, Université Savoie Mont-Blanc/CNRS, 73376 Le Bourget-du-Lac Cedex, France*

[c] *Geology & Geophysics Department, Indian Institute of Technology, Kharagpur, India*

[d] *Tri-Chandra Multiple Campus, Tribhuvan University, Nepal*

[e] *Geological Studies Unit, Indian Statistical Institute, Kolkata 700108, India*

Key words: Himalayan mountain Front, blind thrusts, geomorphology, passive seismic records, Horizontal-to-Vertical Spectral Ratio

Statement of significance: Active tectonics necessitate to select key zones for detailed studies. In the Himalaya, and specially in its piedmont, the quality of natural outcrops is poor due to strong weathering, heavy vegetation and/or anthropic influence. In this paper, we show that the HVSR (Horizontal-to-Vertical Spectral Ratio) method allows exploring the structures beneath the plain south of the Himalayan mountain front. This method is easy to apply in any context and we show that it has allowed revealing the subsurface structures down to 600 meters even in jungle areas. We have correlated geomorphologic scarps evidenced by geomorphologic profiles but nearly invisible in the jungle, to thrust structures evidenced at depth. Two of these scarps of about ten meters affect the 3.7 ± 0.7 ka old surface and imply that about half of the convergence is expressed south of the Himalayan front in this zone.

Abstract

The pattern of active deformation of frontal structures in Darjeeling Himalaya is complex with out-of-sequence reactivations in the chain and development of scarps associated to earthquake ruptures reaching the surface in the piedmont. To clarify the distribution of active deformation in this area, we analyze passive seismic records by the Horizontal-to-Vertical Spectral Ratio method along three NS trending profiles. We image the Siwalik sedimentary rocks / recent deposits interface under the piedmont and show folded and faulted geometries. Two of these faults are located under scarps of about ten meters affecting the 3.7 ± 0.7 ka old surface of the Tista megafan. Such features imply that about half of the convergence is expressed south of the Himalayan front while the other part occurs out-of-sequence in the chain, suggesting a very limited activity of the Main Frontal Thrust (MFT) itself.

1. Introduction

Studying active tectonics in the Himalayas is of primary importance to assess the seismic hazard related to Himalayan earthquakes that overpass Mw 8 (Bilham, 2019). Indeed, Himalayan tectonics follow a rather simple seismic cycle and display a succession of ruptures along the MHT (Main Himalayan Thrust) that transfer most of the Himalayan convergence to the mountain front during great earthquakes (Bilham, 2019). Therefore, the ~20 mm/yr Holocene shortening is frequently considered as almost entirely concentrated at the front of the Himalayan range (e.g., Lavé and Avouac, 2000) and trenches are performed through the MFT (Main Frontal Thrust), the southern emergent tip of the MHT. While trenching is an effective method for reconstructing the calendar of paleo-earthquakes (e.g., Bollinger et al., 2014) and constraining paleoseismic features, it is often difficult to localize the emergence of ruptures and the use of preliminary geophysical acquisition methods is necessary to correctly

50 establish the location of paleoseismic trenches. Subsurface structures of the plain south of the
51 Himalayan front have already been imaged by seismic reflection in the first kilometres of
52 sediments (e.g., Almeida et al., 2018; Bashyal, 1998) and GPR (Ground Penetrating Radar)
53 documenting 10-20 m depth around fault scarps (Pati et al., 2012).

54 The objective of this paper is to show the possibility of imaging subsurface structures
55 down to depths of a few hundred meters, using the geophysical Horizontal-to-Vertical
56 Spectral Ratio (HVSR) method (Bard, 1999; Nakamura, 1989). We apply this method in the
57 piedmont of Darjeeling Himalaya (India) where the pattern of active deformation is especially
58 complex (Figure 1). In this area, out-of-sequence reactivations occur in the chain (Mukul,
59 2000) while recent deformation in the piedmont is distributed over several faults (e.g., Nakata,
60 1989). Our study from HVSR analysis of passive seismic records therefore localizes
61 subsurface structures allowing a better understanding of the active deformation distribution.

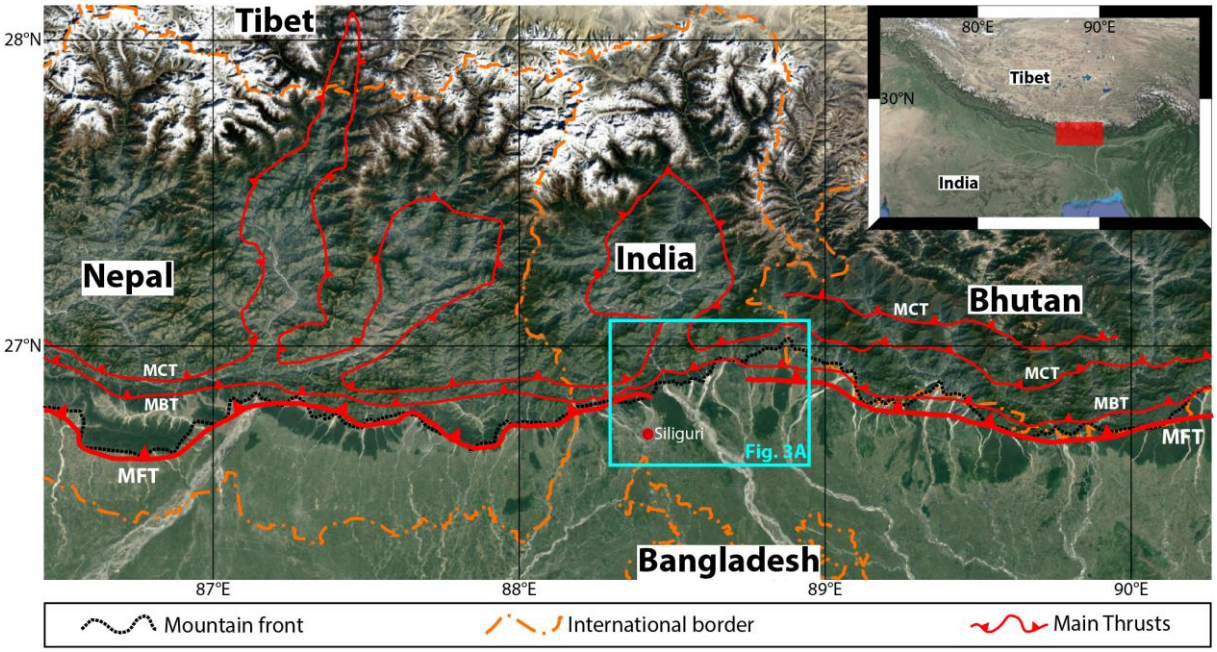

62 *Figure 1: Overview of the study area. Top right inset shows by a red box the location of the map in the*
63 *Himalayan range. Blue box shows location of Figure 3A. Main thrusts of the Himalayan fault system*
64 *shown in red: MCT : Main Central Thrust; MBT : Main Boundary thrust; MFT : Main Frontal Thrust.*
65 *Locations of thrusts are from Tobgay et al. (2012) in Bhutan, Abrahami et al. (2018) in India and*
66 *Mugnier et al. (2011) in Nepal.*
67

2. Horizontal-to-Vertical Spectral ratio analysis of passive seismic records

Methods using seismic noise have been broadly used in the past decades for soil structure exploration (Guéguen et al., 2007; Hinzen et al., 2004; Paudyal et al., 2012), risk assessment (Bhandary et al., 2014), landslide characterization (Méric et al., 2007), building assessment (e.g., Guillier et al., 2014) and even for the exploration of Mars (Knapmeyer-Endrun et al., 2017). The HVSR method consists of using the seismic ambient noise vibrations (Stehly et al., 2006) recorded at a single station from which the ratio between the Fourier amplitude spectra of the horizontal (averaging NS and EW components) to vertical components are estimated.

The seismic noise recordings were collected using a Cityshark II station connected to a 5 s. Lennartz seismometer allowing to perform frequency analysis down to 0.2 Hz (Guillier et al., 2008). The sample frequency was set to 200 Hz with a duration of acquisition between 15 and 30 minutes (description of the data in Appendix A: Supplementary data). For this study, the geopsy open-source pack software was used (www.geopsy.org; Wathelet et al., 2020). The different recordings were processed using 50 s time windows, with a 5 % Tukey taper applied to both ends of each window and the individual HVSR curves were smoothed using the Konno and Ohmachi (1998) method with a constant of 40 before the computing of the final HVSR curve. As the frontal basin is very extended, we use a 1D model for the interpretation of the HVSR.

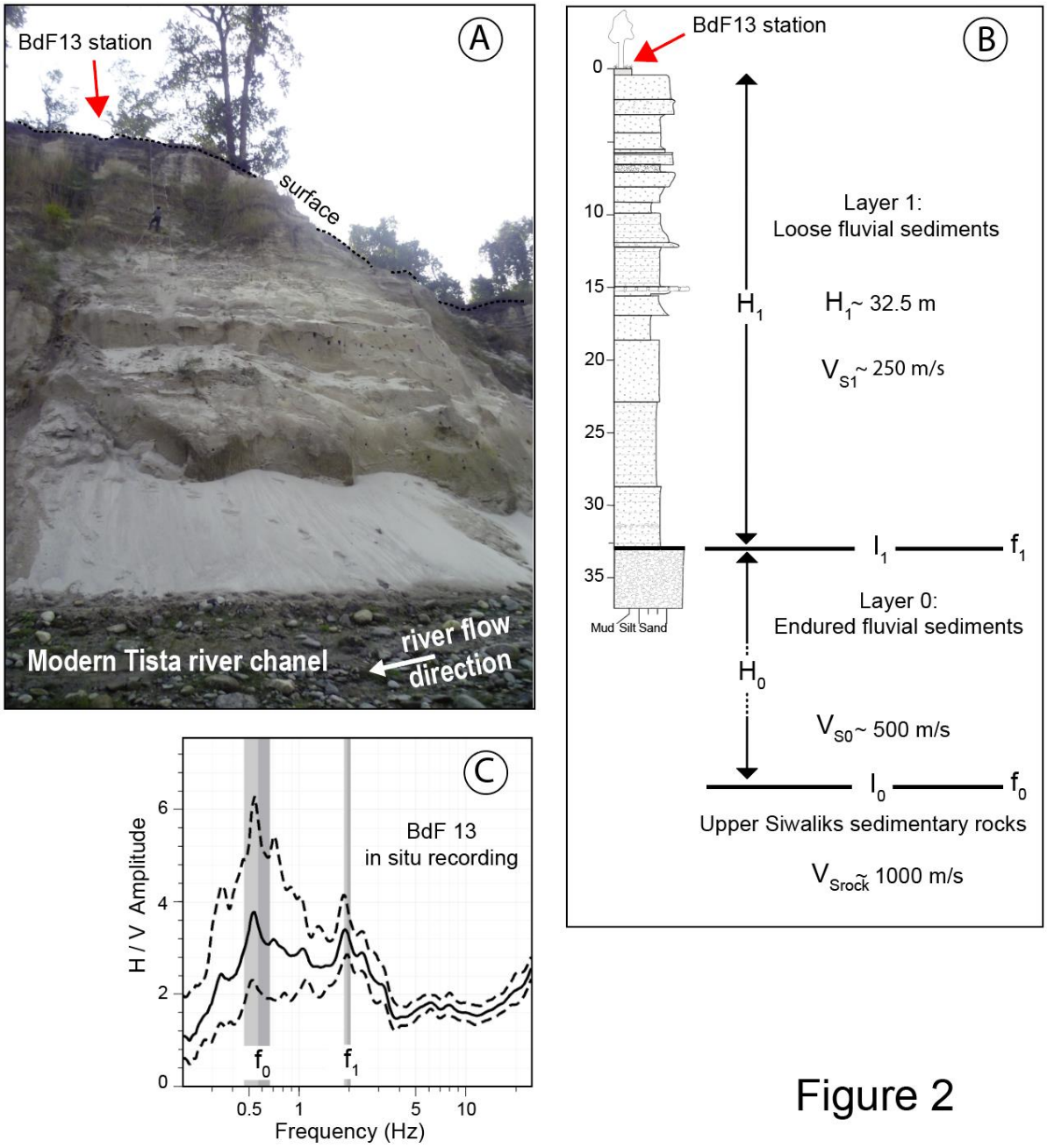

Figure 2

Figure 2: An example of foreland outcrops and of Horizontal-to-Vertical Spectral Ratio (HVSR) acquisition. (A) Picture of the incised sediment deposits of the Tista River (Darjeeling, Siliguri area). The red arrow refers to the location of the ambient vibration recording station (See Figure 2C). (B) Sedimentary log of the megafan incised by the Tista River. (C) Graph of the H/V spectral ratio amplitude versus frequency. The lowest frequency peak (f_0) is linked to the interface (I_0) between endured fluvial sediments and Upper Siwaliks sediments whereas the highest frequency peak (f_1) is linked to the interface (I_1) between loose fluvial sediments and endured fluvial sediments. Width of the light and dark gray bars on f_o and f_1 indicate the standard deviation. From the measured height H_1 of the cliff and the recorded frequency f_1, we calculated the velocity V_{S1}.

From each in situ recording, we obtain a HVSR curve (Figure 2C) from which one or two peaks are extracted: the fundamental frequency of the site (f_0) which is at the lowest frequency (following the recommendations of the SESAME project, in Bard, 2008) corresponding to the deeper interface and when existing, a higher frequency (f_1) corresponding to a shallower interface. The determination of the main frequencies (f_0 and f_1) on the HVSR curve is automatically done by the *geopsy* software. The amplitudes of the peaks are directly linked to the difference of Shear-wave velocity (impedance contrast) at a lithological interface. From SESAME guidelines, a peak can be identified on a HVSR curve only if its amplitude is higher than 2.0, meaning that the impedance contrast between the two layers permits the peak development (Albarello and Lunedei, 2013). Lower peaks are generally discarded. However, those with an amplitude slightly under 2.0 can be considered when there is a spatial continuity in the data, which means that these peaks can represent an interesting interface.

If the HVSR curve displays only one peak, f_0 corresponds to the interface between a superficial layer and a stiffer sediment layer whatever the thickness of this layer. It is then possible to apply eq. (1) and get the depth of the interface (H) from the peak frequency (f_x) and the Shear-wave velocity (Vs) (Hinzen et al., 2004):

$$H = Vs / (4*f_x) \qquad (1)$$

If two peaks are identified on the HVSR curve (Figure 2), the f_1 peak is interpreted as the interface between a superficial loose layer, the thickness of which is directly calculated from eq (1), and a stiffer sediment layer. The f_0 peak characterizes the interface between the second sediment layer located below the superficial layer and a third stiffer rock layer. The thickness of this layer is estimated from the HVSR curve best fitting SH transfer function (SH being the Shear-wave polarized in the horizontal plane) that is obtained from modeling with different thicknesses.

123 For the above calculations, we need at least the surface S-wave velocity. These data
124 are obtained uncommonly from drilling and assumptions usually have to be made that depend
125 on the lithology of the overlaying sediments, their compaction and burial depth. In this study,
126 we performed an ambient seismic noise recording on a cliff where the superficial boundary
127 (i.e., the interface I_1 between loose sands and a conglomeratic endured layer; see Figures 2A
128 and 2B) was outcropping, therefore providing the height H_1 of the upmost sand layer. From
129 the depth H_1 of ~ 32.5 m and the frequency f_1 of ~ 1.9 Hz recorded from this layer (Figure
130 2C), we calculated a corresponding Vs_1 of 250 m/s (eq. 1). As peak interfaces (I_1 and I_0) are
131 well expressed, the S-waves velocity of the two underlying layers Vs_0 and Vs_{rock} were
132 respectively estimated at about 500 m/s and ≥ 1000 m/s respectively and Vs_{rock} probably
133 corresponds to the Siwalik sedimentary rocks.

134 In the following, it is assumed in the case of a single peak on the HVSR curve, that the
135 S-wave velocity down to the Siwalik sedimentary rocks is of 500 m/s, allowing to derive
136 directly the thickness and standard deviation of the upper layer from f_0. For double peak
137 HVSR curves (Figure 2C), it is assumed that Vs_{rock} = 1000 m/s, Vs_0 = 500 m/s and Vs_1 = 250
138 m/s and we derived H_1 ($\pm\boldsymbol{\sigma}$) from f_1 using eq. (1). We then proceeded by SH transfer function
139 modeling (Wathelet et al., 2020): H_1 ($\pm\boldsymbol{\sigma}$), Vs_1 and Vs_0 are known (Vp/Vs is assumed as 2.0),
140 so we compute the SH transfer function with different thicknesses, conserving the models
141 with a lower frequency peak fitting in a f_0 ± sigma range. This leads to an averaged thickness
142 (H_0) with a standard deviation.

143 From the ambient seismic data acquired along the Tista and Gish rivers and their
144 processing, we calculated the depth of the peak interfaces on a large area south of the
145 mountain front and extracted the geometry of the underlying structures.

146

147

148 **3. Results**

149 **3.1 Location of the acquisition**

150 We conducted a subsurface analysis using the HVSR method in the Siliguri area, south
151 of the Darjeeling Himalaya. There, the Himalayan mountain front is sinuous (Figure 3A) and
152 characterized by the major Dharan salient and Gorubathan recess separated by the main Gish
153 Transverse Fault (GTF). The Quaternary alluvia are in contact with synorogenic sedimentary
154 rocks of the Siwalik group in the Dharan salient or with pre-orogenic rocks in the Gorubathan
155 recess. East of the GTF, several active faults were described (Srivastava et al., 2017 and
156 references therein): the MBT (Main Boundary Thrust), MFT and Bharadighi back-thrust
157 (Figure 1). Another fault (the Batabari fault) between the MFT and Bharadighi fault was also
158 inferred from river morphology. West of the GTF, the location of the active faults is still under
159 discussion (Jayangondaperumal, personal communication). Our field observations showed
160 that the late Quaternary alluvium of the Tista River (Abrahami et al., 2018) onlaps the
161 Siwaliks and seals the MFT, therefore suggesting that the MFT is not active since several
162 kyrs. In contrast geomorphologic markers suggest that the MBT fault system is still active
163 (Mukul, 2000) in the Dharan salient. The Tista megafan ahead of the Himalayan front is
164 strongly incised –about 37m– and the origin of this incision is still debated – climatic or
165 tectonically driven (Abrahami et al., 2018). Due to the strong vegetal cover of the area,
166 geomorphologic studies are difficult although preliminary RTKGNSS profiles (Figure 4)
167 suggest that scarps would affect the top of the Tista megafan dated at 3.7 ± 7 ka (Abrahami et
168 al., 2018). The HVSR method is therefore used to image the geometry of the structures
169 beneath the Tista megafan and determine the origin of its incision.

170

171

172

3.2 Subsurface structures inferred from HVSR method

The passive seismic data were acquired along three approximately N-S trending profiles (Figure 3A) located on the Tista megafan (profiles Siliguri and Tista, respectively 17 and 23 recording sites) and the Gish Fan (profile Gish, 13 recording sites).

The results of the HVSR method show peaks of the H/V ratio at two different frequencies in about 80% of the locations (Figure 3B), therefore indicating two interfaces with contrasted S-wave velocities and three distinct layers. Following the method section, interface (I_1) was attributed to a superficial contact within the Quaternary deposits (velocity contrast Vs_1/Vs_0) and interface (I_0) to the contact between Quaternary sediments and the Neogene Siwalik sedimentary rocks (velocity contrast Vs_0/Vs_{rock}) (Figures 2 and 3). The (I_1) shallowest interface (grey dots) presents depths of a few meters to a few tens of meters. The (I_0) deeper interface (orange dots) displays depths varying from ~100 to 600 m below the surface and globally dips southwards. Very close to the mountain front, it shows a complex pattern and its depth locally changes abruptly (Figure 3B).

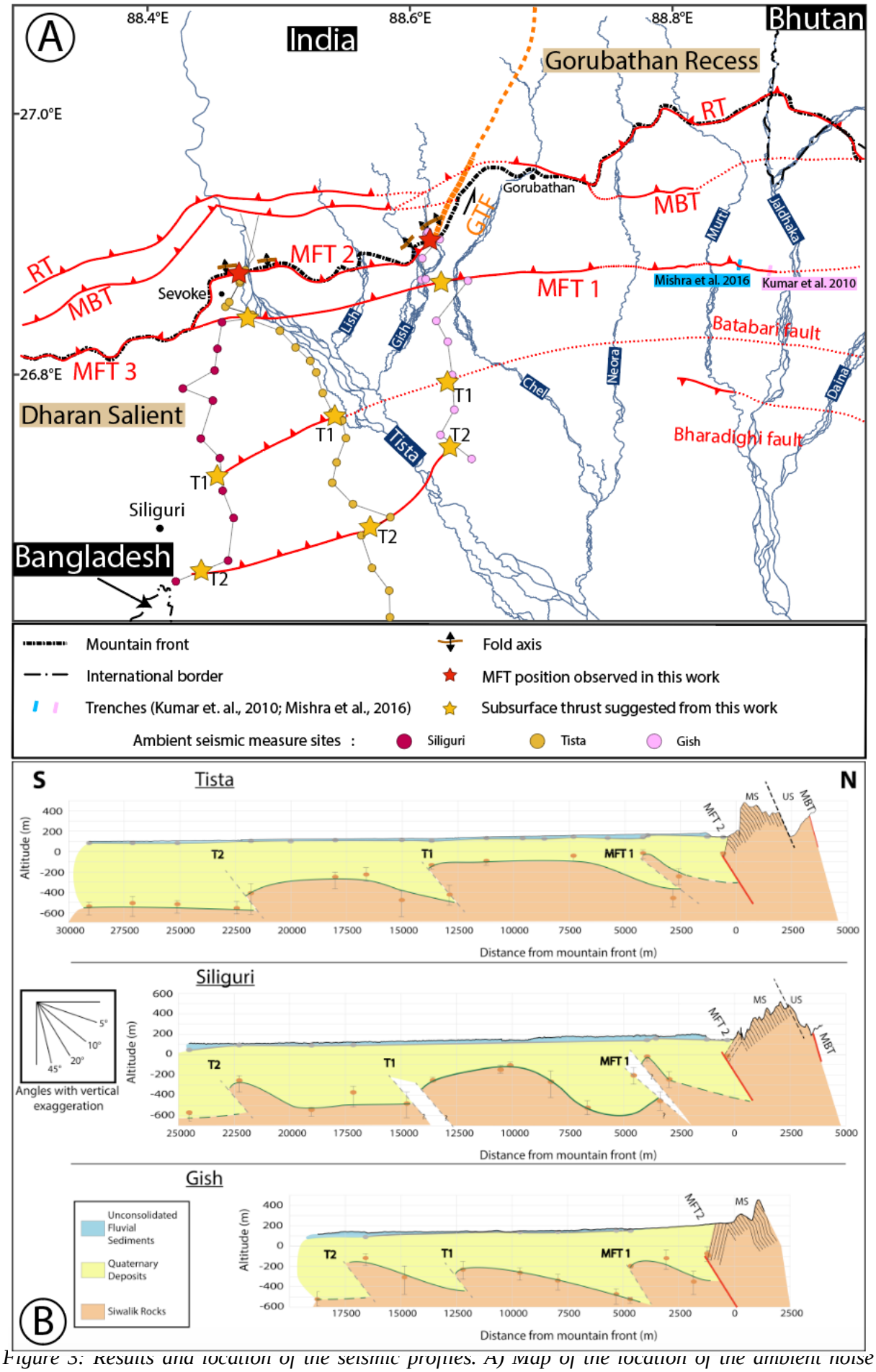

Figure 3: Results and location of the seismic profiles. A) Map of the location of the ambient noise

seismic lines put back in the regional tectonic context. The Gish Transverse Fault (GTF) separates the western Dharan salient from the eastern Gorubathan recess and is indicated by the orange line. Thrusts are represented in red. East of the GTF, the MBT, MFT1 and Bharadighi fault are from Nakata (1989). RT (Ramgarh Thrust) and Batabari fault are from Srivastava et al. (2017). West of the GTF, MFT1, T1 and T2 are suggested from HVSR geophysical data (see Figure 3B). MFT2 and MFT3 are respectively from personal field work, and Jayangondaperumal (personal communication), MBT and RT are from Mukul (2010). See "Fig3A_supporting information.kmz" for location of the profiles with the google earth software; B) Ambient seismic data (See the data in "Fig3B_Supporting Information.xls") from the Darjeeling area and their interpretation. Location of the data on figure 3A. Dips of the Neogene Siwalik strata along the Gish and Tista sections are from our own data and Acharyya et al., (1987). Grey points correspond to the (I_1) interface within Quaternary deposits, orange points and green lines correspond to the (I_0) interface which is interpreted as the Quaternary/Siwaliks contact. Suggested thrusts are represented in dashed gray lines. Note that the vertical scale is strongly exaggerated and the bottom left inset indicates the real values of the dips.

4. Discussion

4.1 Interpretation of the HVSR data and comparison with the Tista megafan morphology

The interpretation of the HVSR data (Figures 3 and 4D) infers that the top of the Siwaliks rocks is affected by thrusts and folds, a structuration already imaged by seismic reflections beneath the piedmont of East-Central Himalaya (Bashyal, 1998), where the thrust faults branch off the same basal decollement as the MFT. The interpretation assumes that MFT and other thrust faults dip ~20° northward (Almeida et al., 2018) and that the folds associated to the blind thrusts have asymmetrical limbs, by analogy with the fault-related folds observed in the Siwaliks (e.g., Mugnier et al., 1999). Three major thrusts are inferred along each profile (Figure 3B) and their map pattern suggests that the northern thrust is located in the continuity of scarps related to the MFT1 segment in the Gorubathan Recess (Nakata, 1989) and of the MFT3 segments in the Dharan Salient (Figure 3A). The T1 fault could be in the continuity of the Batabari fault defined by Srivastava et al. (2017).

This interpretation suggests that two scarps that are evidenced by geomorphologic profiles but nearly invisible in the jungle and that affect the Tista megafan (Figure 4C) with a total offset of ~ 18 ± 2m (Figures 4A and 4B), would be related to the activity of the T1 and T2 thrusts. Similar fault scarps, but more pronounced in height, were also evidenced eastward in the Gorubathan Recess piedmont and were found associated to the surface ruptures of ~ A.D. 1100 (Kumar et al., 2010) and/or A.D. 1255 (Mishra et al., 2016) earthquakes (location on Figure 1). The two escarpments along the Tista profile could be linked to earthquakes occurring since the abandonment of the upper surface of the fan, dated at 3.7 ±0.7 kyrs. About twenty meters of the Tista megafan incision is then linked to uplift along the faults related to these scarps and the rest of the 37 m could be due to climatic fluctuations (Abrahami et al., 2018) or to more distributed uplift. Therefore, the mean uplift associated to the Tista megafan is at least 4.9 ± 1.6 mm.yr^{-1}. Taking into account the structural studies of fault scarps (e.g., Jayangondaperumal et al., 2013), the slip beneath a scarp is at least twice the uplift, and the shortening absorbed in this part of the Himalayan piedmont would therefore be approximately 10 mm.yr-1, i.e., about half of the estimated Himalayan convergence (e.g., Lavé and Avouac, 2000).

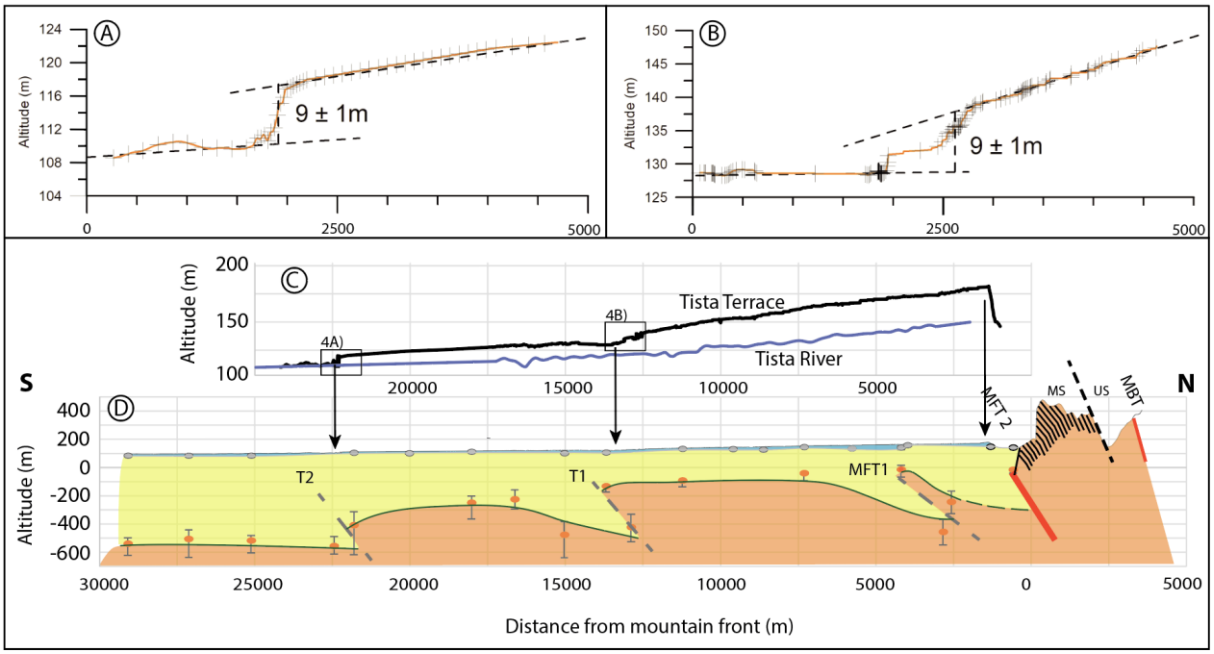

Figure 4: Comparison of topographic profiles and geophysical images of the structures in the Tista megafan. A) Topographic profile through the southern scarp; B) Topographic profile through the northern scarp; in brown, profile from a weighted average of 20 RTKGNSS (Real-Time Kinematic Global Network Satellite System) data; C) Topographic profile through the Tista fan (from our RTKGNSS data). Black rectangles refer to the location of scarps of figures 4A and 4B; D) Inferred structures at depth from ambient seismic data (Tista profile of Figure 3).

4.2 Limits and utility of the HVSR method

We demonstrate that the HVSR method is a very powerful and simple tool that helps imaging the subsurface structures. In the case of the Darjeeling piedmont, our work allows a better mapping of the complex thrust network and shows that about half of the active tectonics is distributed along several thrusts ahead of the Himalayan front. Nonetheless, the HVSR method only records the major interfaces characterized by strong velocity contrasts and does not furnish a detailed picture of the structures. We therefore suggest that this method is only useful for preliminary mapping studies. It may indicate the key zones where more detailed surficial studies, such as GPR or trenching can be performed and allows to relate them with regional deeper structures, therefore improving the general knowledge of the Himalayan

252 tectonics. Finally, it participates in identifying the active structures and is therefore of the
253 upmost importance for assessing seismic hazard in densely populated regions.

254 **Acknowledgments:**

255 We acknowledge A. De Leeuw for numerous constructive discussions. We thank Dr.
256 Sandip More for field assistance. This work has been funded by CNRS Himal-Fan ANR-
257 17-CE01-0018 and in 2019 by an internal grant of the Institut des Sciences de la Terre
258 (Grenoble). Maps were performed using the free Geographic Information System
259 (www.qgis.org).

260

261 **Declaration of Competing Interest:**

262 We hereby declare that we do not have any conflict of interest.

263 **Data availability statement:**

264 The data supporting the findings of this study are available on:
265 - Precise location of the passive seismic record sites in "Fig3A_Supporting Information.kmz"
266 - Geophysical parameters and depths of the interface at each passive seismic record sites in
267 "Fig3B_Supporting Information.xls"
268 - For the others data, they may be sent on request by the corresponding author.
269

270 **REFERENCES:**

Abrahami, R., Huyghe, P., Van der Beek, P., Lowick, S., Carcaillet, J., Chakraborty, T., 2018. Late Pleistocene – Holocene development of the Tista megafan (West Bengal, India): 10Be cosmogenic and IRSL age constraints. Quat. Sci. Rev. 185, 69–90. doi: 10.1016/j.quascirev.2018.02.001

Acharyya, S.K., Bhatt, D.K., Sen, M.K., 1987. Earliest Miocene planktonic foraminifera from Kalijhora area, Tista river section, Darjeeling Sub-Himalaya. Indian Minerals 41, 31–37.

Albarello, D., Lunedei, E., 2013. Combining horizontal ambient vibration components for H/V spectral ratio estimates. Geophys. J. Int. 194, 936–951. doi: 10.1093/gji/ggt130

271 Almeida, R.V., Hubbard, J., Liberty, L., Foster, A., Sapkota, S.N., 2018. Seismic imaging of the
272 Main Frontal Thrust in Nepal reveals a shallow décollement and blind thrusting. Earth
273 Planet. Sci. Lett. 494, 216–225. doi: 10.1016/j.epsl.2018.04.045

Bard, P.-Y., 1999. Microtremor measurements: a tool for site effect estimation. The effects of surface geology on seismic motion, Irikura, Kudo, Okada & Sasatani (eds) 3, 1251–1279.

Bard, P.-Y., 2008. Foreword: The H/V technique: capabilities and limitations based on the results of the SESAME project. Bull. Earthq. Eng. 6, 1–2. doi: 10.1007/s10518-008-9059-4Bashyal, R.P., 1998. Petroleum exploration in Nepal. Journal of Nepal Geological Society 19–24.

Bhandary, N.P., Yatabe, R., Yamamoto, K., Paudyal, Y.R., 2014. Use of a Sparse Geo-Info Database and Ambient Ground Vibration Survey in Earthquake Disaster Risk Study – A Case of Kathmandu Valley. J. Civ. Eng. Res. 4, 20–30. doi: 10.5923/c.jce.201402.03

Bilham, R., 2019. Himalayan earthquakes: a review of historical seismicity and early 21st century slip potential. Geol. Soc. Lon. Spec. Publ. 483, 423–482. doi: 10.1144/SP483.16

Bollinger, L., Sapkota, S.N., Tapponnier, P., Klinger, Y., Rizza, M., Van der Woerd, J., Tiwari, D.R., Pandey, R., Bitri, A., Bes de Berc, S., 2014. Estimating the return times of great Himalayan earthquakes in eastern Nepal: Evidence from the Patu and Bardibas strands of the Main Frontal Thrust: Return period of Himalayan earthquakes. J. Geophys. Res. Solid Earth 119, 7123–7163. doi: 10.1002/2014JB010970

Guéguen, P., Cornou, C., Garambois, S., Banton, J., 2007. On the Limitation of the H/V Spectral Ratio Using Seismic Noise as an Exploration Tool: Application to the Grenoble Valley (France), a Small Apex Ratio Basin. Pure Appl. Geophys. 164, 115–134. doi: 10.1007/s00024-006-0151-x

Guillier, B., Atakan, K., Chatelain, J.-L., Havskov, J., Ohrnberger, M., Cara, F., Duval, A.-M., Zacharopoulos, S., Teves-Costa, P., The SESAME Team, 2008. Influence of instruments on the H/V spectral ratios of ambient vibrations. Bull. Earthquake Eng. 6, 3–31. doi: 10.1007/s10518-007-9039-0

Guillier, B., Chatelain, J.-L., Tavera, H., Perfettini, H., Ochoa, A., Herrera, B., 2014. Establishing Empirical Period Formula for RC Buildings in Lima, Peru: Evidence for the Impact of Both the 1974 Lima Earthquake and the Application of the Peruvian Seismic Code on High-Rise Buildings. Seismol. Res. Lett. 85, 1308–1315. doi: 10.1785/0220140078

Hinzen, K.-G., Weber, B., Scherbaum, F., 2004. On the resolution of H/V measurements to determine sediment thickness, a case study across a normal fault in the Lower Rhine Embayment, Germany. J. Earth. Eng. 08, 909–926. doi: 10.1142/S136324690400178X

Jayangondaperumal, R., Mugnier, J.L., Dubey, A. K., 2013. Earthquake slip estimation from the scarp geometry of Himalayan Frontal Thrust, western Himalaya: Implications for seismic hazard assessment, Int. J. Earth Sci.. doi : 10.1007/s00531-013-0888-2

Knapmeyer-Endrun, B., Golombek, M.P., Ohrnberger, M., 2017. Rayleigh Wave Ellipticity Modeling and Inversion for Shallow Structure at the Proposed InSight Landing Site in Elysium Planitia, Mars. Space Sci. Rev. 211, 339–382. doi: 10.1007/s11214-016-0300-1

Konno, K., Ohmachi, T., 1998. Ground-motion characteristics estimated from spectral ratio between horizontal and vertical components of microtremor. Bull. Seismol. Soc. Am. 88, 228–241.

Kumar, S., Wesnousky, S.G., Jayangondaperumal, R., Nakata, T., Kumahara, Y., Singh, V., 2010. Paleoseismological evidence of surface faulting along the northeastern Himalayan front, India: Timing, size, and spatial extent of great earthquakes. J. Geophys. Res. 115, B12422. doi: 10.1029/2009JB006789

Lavé, J., Avouac, J.P., 2000. Active folding of fluvial terraces across the Siwaliks Hills, Himalayas of central Nepal. J. Geophys. Res. 105, 5735–5770. doi: 10.1029/1999JB900292

Méric, O., Garambois, S., Malet, J.-P., Cadet, H., Guéguen, P., Jongmans, D., 2007. Seismic noise-based methods for soft-rock landslide characterization. Bull. Soc. Géol. Fr. 178, 137–148. doi: 10.2113/gssgfbull.178.2.137

Mishra, R.L., Singh, I., Pandey, A., Rao, P.S., Sahoo, H.K., Jayangondaperumal, R., 2016. Paleoseismic evidence of a giant medieval earthquake in the eastern Himalaya: Rupture Length of A.D. 1255 Earthquake. Geophys. Res. Lett. 43, 5707–5715. doi: 10.1002/2016GL068739

Mukul, M., 2000. The geometry and kinematics of the Main Boundary Thrust and related neotectonics in the Darjiling Himalayan fold-and-thrust belt, West Bengal, India. J. Struct. Geol. 22, 1261–1283. doi: 10.1016/S0191-8141(00)00032-8

Mukul, M., 2010. First-order kinematics of wedge-scale active Himalayan deformation: Insights from Darjiling–Sikkim–Tibet (DaSiT) wedge. J. Asian Earth Sci. 39, 645–657. doi: 10.1016/j.jseaes.2010.04.029

Mugnier, J.L., Huyghe, P., Gajurel, A.P., Upreti, B.N., Jouanne, F., 2011. Seismites in the Kathmandu basin and seismic hazard in central Himalaya. Tectonophysics 509, 33–49. https://doi.org/10.1016/j.tecto.2011.05.012

Mugnier, J.L., Leturmy, P., Mascle, G., Huyghe, P., Chalaron, E., Vidal, G., Husson, L., Delcaillau, B., 1999. The Siwaliks of western Nepal. J. Asian Earth Sci. 17, 629–642. doi: 10.1016/S1367-9120(99)00038-3

Nakamura, Y., 1989. A method for dynamic characteristics estimation of subsurface using microtremor on the ground surface. Railway Technical Research Institute, Quarterly Reports 30.

Nakata, T., 1989. Active faults of the Himalaya of India and Nepal. Geol. Soc. Am. pp. 243–264. doi: 10.1130/SPE232-p243

Pati, P., Parkash, B., Awasthi, A.K., Jakhmola, R.P., 2012. Spatial and temporal distribution of inland fans/terminal fans between the Ghaghara and Kosi rivers indicate eastward shift of neotectonic activities along the Himalayan front. A study from parts of the upper and middle Gangetic plains, India. Earth Sci. Rev. 115, 201–216. doi: 10.1016/j.earscirev.2012.10.006

Paudyal, Y.R., Yatabe, R., Bhandary, N.P., Dahal, R.K., 2012. A study of local amplification effect of soil layers on ground motion in the Kathmandu Valley using microtremor analysis. Earthq. Eng. Eng. Vib. 11, 257–268. doi: 10.1007/s11803-012-0115-3

Srivastava, V., Mukul, Manas, Mukul, Malay, 2017. Quaternary deformation in the Gorubathan recess: Insights on the structural and landscape evolution in the frontal Darjiling Himalaya. Quat. Int. 462, 138–161. doi: 10.1016/j.quaint.2017.05.004

Stehly, L., Campillo, M., Shapiro, N.M., 2006. A study of the seismic noise from its long-range correlation properties. J. Geophys. Res. 111, B10306. doi: 10.1029/2005JB004237

Tobgay, T., McQuarrie, N., Long, S., Kohn, M.J., Corrie, S.L., 2012. The age and rate of displacement along the Main Central Thrust in the western Bhutan Himalaya. Earth Planet. Sci. Lett. 319–320, 146–158. https://doi.org/10.1016/j.epsl.2011.12.005

Wathelet, M., Chatelain, J.-L., Cornou, C., Giulio, G.D., Guillier, B., Ohrnberger, M., Savvaidis, A., 2020. Geopsy: A User-Friendly Open-Source Tool Set for Ambient Vibration Processing. Seismol. Res. Lett. 91, 1878–1889. doi: 10.1785/0220190360